Faceting transition of gold nano materials

Yanting Wang

Molecular Dynamics simulations show that macroscopic shape transformations are intimately connected with faceting transition for both icosahedral gold clusters and fcc gold nanorods.

I. INTRODUCTION

Gold nano materials have been of great interest in recent materials research due to their prospective wide range of applications in various area, such as biological sensors and optical equipments. The behaviour of gold nano materials at various temperatures therefore requires close theorectical study.

Gold nanorods with aspect ratio of 3.0 have first been studied by constant temperature Molecular Dynamics (MD). Our results indicate that, during continuous heating from 5K to complete melting, rods with about 10^3-10^4 atoms transform in two stages: a shape transition leading the rods of smaller aspect ratio at lower temperature precedes the melting transition to liquid nanospheres. Structural change of both the surface and interior, as well as surface disordering and reordering, has also been observed during the whole process [1].

In order to study the role of the surface in these transitions with reduced complexity, the geometrical and energetical properties of gold clusters cooled from liquid, for which the icosahedral structure was formed, has been studied at different temperature levels between 100K and 1500K. Our results for a system with 2624 atoms show that, at temperatures as low as about 600K, the vertex atoms start to move around, which rounds the sharp corners of the icosahedral cluster shape. When temperature is higher, edges, then facets, are also rounded out by thermal fluctuation and diffusion of atoms. The facets totally disappear just below the bulk melting temperature. The disappearance of such flat facets is known as the *faceting transition.*

The same analysis methods for icosahedral gold clusters have also been applied to the configurations of gold nanorods. Qualitatively, it has been observed that macroscopic shape transformations are intimately connected with the faceting transition occuring on the sides of the nanorods.

II. METHODS

A. Molecular Dynamics

Molecular Dynamics (MD) simulation employs a classical potential to simulate the evolvement of a many-body system with time. Compared to the more accurate *ab initio* methods which can do simulation work, on today's computers, for the systems with about hundreds of particles, MD can easily handle thousands of particles.

At each time step of MD, the forces among particles are calculated with the many-body potential according to their positions, then the Newton's equations of motion are integrated to obtain the new positions of particles. The gold "glue" potential [2] has been used in our simulations since it's known to be accurate for describing bulk, defect and surface properties of gold. In the "glue" model, the potential energy of a system of N atoms consists of a sum of pair potentials and a many-body "glue" energy:

$$V = \frac{1}{2}\sum_i \sum_{j\neq i} \phi\left(r_{ij}\right) + \sum_i U\left(n_i\right). \tag{1}$$

Here the sums run over all particles, $r_{ij} = |\mathbf{r}_i - \mathbf{r}_j|$ is the interatomic distance between atoms i and j, and $\phi(r)$ is the pair interaction energy. The many-body "glue" energy depends on the coordination numbers n_i defined for all atoms,

$$n_i = \sum_j \rho\left(r_{ij}\right), \tag{2}$$

where $\rho(r)$ is a short-ranged monotonically decreasing function of the interatomic distance r. Cutoffs of 3.9Å for $\rho(r)$ and 3.7Å for $\phi(r)$ are used. The equations of motion are integrated with the velocity Verlet algorithm [3] with a time step of 4.3fs.

The order of computational complexity for looping over all pairs of particles to calculate the forces is N^2. However, because a cutoff distance is present in the glue model, the simulation space can be divide into cells with side length a little larger than the cutoff, and the pair loops are only taken over those pairs in the same cell or neighboring cells. With this so-called *cell index method* the complexity is reduced down to the order of N [3].

Besides MD, the cell index method can also be applied to many data analysis methods, such as bond order parameter calcualtions and cone algorithms, which are described in the following sections.

B. Radius of Gyration

The radius of gyration has been calculated to monitor the shape change of the gold nanorods during the heating process. It is defined as

$$r_g = \sqrt{\frac{1}{N}\sum_i [\mathbf{r}_i(t) - \mathbf{r}_c]^2}, \tag{3}$$

where the sum runs over all particles and $\mathbf{r}_c$ is the center of mass of the rod. The radius of gyration is large for rods with large aspect ratio and reaches its minimum value for spherical shape.

C. Bond-orientational Order Parameters

The structure of crystals can be quantified by bond-orientational order parameters [4]. Bonds are defined as the vectors joining a pair of neighboring particles with the distance less than a cutoff radius (3.8Å in our case). The general idea of bond-orientational order parameters is to capture the symmetry of bond orientations regardless of the bond lengths. Spherical harmonics are employed when calculating bond order parameters.

The local order parameters associated with a bond $\mathbf{r}$ are a set of numbers

$$Q_{lm}(\mathbf{r}) \equiv Y_{lm}(\theta(\mathbf{r}), \phi(\mathbf{r})), \tag{4}$$

where $\theta(\mathbf{r})$ and $\phi(\mathbf{r})$ are the polar and azimuthal angles of the bond with respect to an arbitrary reference frame and $Y_{lm}(\theta(\mathbf{r}), \phi(\mathbf{r}))$ are spherical harmonics. Only even-l spherical harmonics are considered so that they are invariant under inversion. Global bond order parameters can then be calculated by averaging $Q_{lm}(\mathbf{r})$ over all bonds:

$$\overline{Q}_{lm} \equiv \frac{1}{N_b}\sum_{\text{bonds}} Q_{lm}(\mathbf{r}), \tag{5}$$

where N_b is the number of bonds. To make the order parameters invariant with respect to rotations of the reference frame, the second-order invariants are defined as

$$Q_l \equiv \sqrt{\frac{4\pi}{2l+1}\sum_{m=-l}^{l} \left|\overline{Q}_{lm}\right|^2}, \tag{6}$$

and the third-order invariants are defined as

$$W_l \equiv \sum_{m_1,m_2,m_3}^{m_1+m_2+m_3=0} \begin{pmatrix} l & l & l \\ m_1 & m_2 & m_3 \end{pmatrix} \cdot \overline{Q}_{lm_1}\overline{Q}_{lm_2}\overline{Q}_{lm_3}, \tag{7}$$

where the coefficients $(\cdots)$ are the Wigner $3j$ symbols [5]. Furthermore, reduced order parameters, almost independent of the precise definition of nearest neighbors, can be defined as

$$\hat{W}_l \equiv \frac{W_l}{\left(\sum_m |Q_{lm}|^2\right)^{3/2}}. \tag{8}$$

We used the four bond order parameters Q_4, Q_6, $\hat{W}_4$ and $\hat{W}_6$ to identify structures accurately. The values of these bond order parameters for fcc, hcp, icosahedral, and liquid structures are listed in Tab.I.

Global bond order parameters averaging over all the bonds monitor the macroscopic structural change, while local bond order parameters taking in only bonds associated with a specific pariticle identify the local structure of this particle.

TABLE I: Bond order parameters for face-centered-cubic (fcc), hexagonal close-packed (hcp), icosahedral and liquid structures.

Geometry	Q_4	Q_6	$\hat{W}_4$	$\hat{W}_6$
fcc	0.19094	0.57452	-0.159317	-0.013161
hcp	0.09722	0.48476	0.134097	-0.012442
icosahedral	0	0.66332	0	-0.169754
liquid	0	0	0	0

D. Cone Algorithm

A cone algorithm has been developed to discriminate surface particles accurately according to their geometrical positions. As shown in Fig. 1, for a given particle, if there exists at least one *hollow cone* region with its vetex on the given particle, so that no other particles inside it, this given particle is a surface particle. The side length a and the angle θ of the cone are two adjustable parameters of this algorithm. By visual examination of the generated surface configurations, we determined the parameters as $a = 5.0$Å and $\theta = \frac{\pi}{3}$ for our case.

Cone algorithm can be used recursively to strip particles out layer by layer.

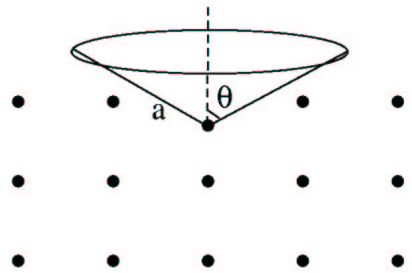

FIG. 1: Scheme of a *hollow cone* defined in the cone algorithm.

E. Local Curvature Fitting

In order to quantify surface roughness (flatness), the local surface geometry for a given surface particle with nearest neighoring surface particles should be fitted with a ellipsoid to find out its two principle axis and radii (thus local curvatures) (Fig. 2). To linearize this problem, the normal vector of the ellipsoid is first determined by fitting the

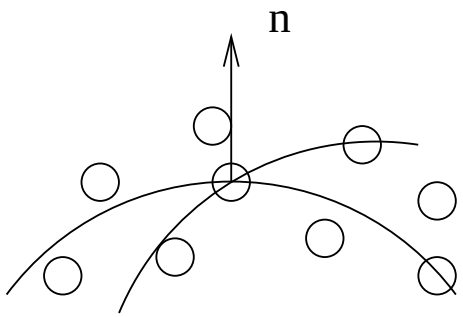

FIG. 2: Scheme of local curvature fitting.

optimized plane to this local surface structure and taking the normal vector of this plane as that of the ellipsoid. We

define the *discrete differential roughness* of a local structure as:

$$D = \sqrt{\frac{\sum_i d_i^2}{N}}, \tag{9}$$

where N is the number of particles, and d_i, $i = 1 \ldots N$ is the distance from the ith particle to the tangent plane:

$$d_i = \mathbf{n} \cdot (\mathbf{r}_i - \mathbf{r}_0). \tag{10}$$

Here $\mathbf{n}$ is the (unsolved) normal vector of the tangent plane, $\mathbf{r}_i$ is the coordinate of the ith particle, $\mathbf{r}_0$ is the coordinate of the reference point, which is the center of mass in our case.

To solve the normal vector is actually a symmetric eigenvalue problem if an undetermined Lagrange multiplier λ is used:

$$\frac{\delta}{\delta \mathbf{n}} \left[\sum_i d_i^2 - \lambda \left(\mathbf{n}^2 - 1 \right) \right] = 0. \tag{11}$$

Once the normal vector $\mathbf{n}$ is fixed, we can assign two arbitrary local vectors $\mathbf{e}_x$ and $\mathbf{e}_y$ diagonized with $\mathbf{n}$ and each other. We then map the coordinates of the particles to this new coordinate system $\mathbf{e} \equiv (\mathbf{e}_x, \mathbf{e}_y, \mathbf{n})$:

$$\mathbf{x}_i = (\mathbf{q}_i - \mathbf{q}_0) \cdot \mathbf{e}, \tag{12}$$

where $\mathbf{q}_i$, $i = 1 \ldots N$ is the old coordinate of ith particle, $\mathbf{x}_i \equiv (x_i, y_i, z_i)$ is the new coordinate, $\mathbf{q}_0$ is the reference point, which is the particle itself in this case.

Define parabolic fit function:

$$f(x, y) = a_{xx} x^2 + 2 a_{xy} xy + a_{yy} y^2, \tag{13}$$

and minimize

$$S = \sum_i \left(z_i - f(x_i, y_i) \right)^2, \tag{14}$$

with respect to a_{xx}, a_{xy}, and a_{yy}. Diagonizing the symmetric matrix of a_{xx}, a_{xy}, and a_{yy} gives the two principle axis and the corresponding local curvatures.

F. Mean Squared Displacements

Mean squared displacement is a convenient way to show the average ability of movement for a group of atoms. It is defined as

$$MSD(\Delta t) = \frac{1}{MN} \sum_{j=1}^{M} \sum_{i=1}^{N} \left(\mathbf{r}_i(t_j + \Delta t) - \mathbf{r}_i(t_j) \right)^2, \tag{15}$$

where $\mathbf{r}$ is the position of the atom, N is the number of atoms, Δt is the time interval, M is the number of time intervals, which are chosen to be independent with each other.

III. RESULTS

A. Shape and Melting Transitions of Gold Nanorods

As initial structure for our simulations we construct a nanorod with the geometry of the gold nanorods studied experimentally by Wang *et al.* [6]. These rods have an aspect ratio of 3.0 and their sides consist of four large {100} and four large {110} facets oriented parallel to the rod axis. Each end has a {001} facet and four small {111} facets connecting the {110} and the {001} facets, and four small {110} facets connecting the {100} and the {001} facets. The gold nanorods with such surfaces were carved out from the bulk gold with a pure fcc structure. A rod with 11076 atoms is shown in Fig. 3.

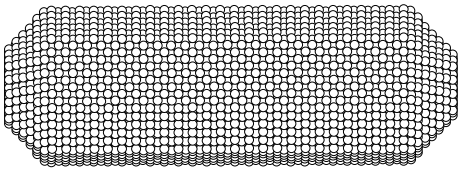

FIG. 3: The gold nanorod with 11076 atoms carved out from the fcc bulk gold.

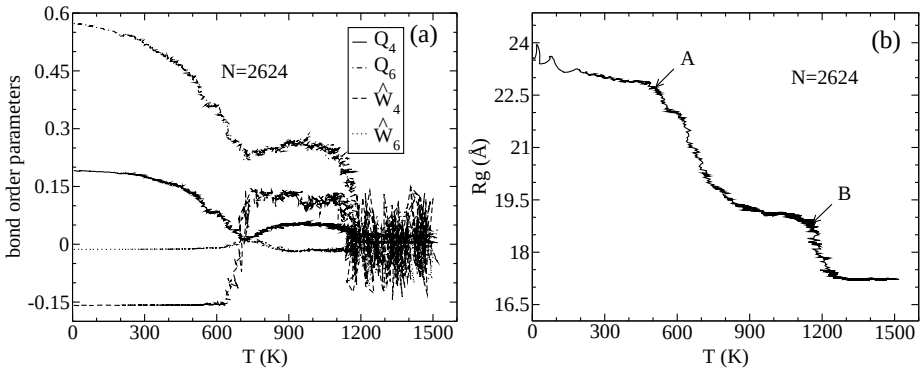

FIG. 4: Temperature dependence of the average bond order parameters a) and the radius of gyration b) for the gold nanorod with 2624 atoms during continuous heating.

The gold nanorod with 2624 atoms has been heated from 5K to complete melting by constant temperature MD. The time step is 4.3fs. At each MD step the kinetic energy of the system is increased by a fixed amount so that the heating rate is 7×10^{12}K/s. Fig. 4 indicates that both shape and structural changes illustrate that there has a shape transition before the melting transition. The shorter and wider intermediate rod generated by the shape transition has an aspect ratio of 1.8 and exists for a wide range of temperature. Equilibrium (constant energy) MD simulations taken on the instantaneous configurations of this intermediate state at 743K, 905K and 1033K show that they were stable for more than 400ps.

The same simulations have also been taken for the rods with the same aspect ratio but different sizes of 1404, 2094, 3610, 4960, 5870, 7552, 9678 and 11076 atoms. Similar phenomena have been observed in all of the simulations.

Local bond order parameters have been calculated to look closer at the structural change of the rod. The local bond order parameter calculations have been taken our for each atom according to the geometry constructed by its nearest neighbor atoms. Fig. 5 show the results of local bond order parameters analysis.

These results indicate that the shape transition is accompanied by an internal structural change from fcc-dominated to hcp-dominated. Further heating causes these intermediate wider rods to melt and the rods become disordered collapsing to spherical shape. Reordering of the internal atoms occurs shortly before melting. They are coincident with the experimental observations of a) shorter and wider and ϕ-shaped intermediate particles [7, 8] and b) internal point and planar defects [9].

B. Faceting Transition of Icosahedral Gold Clusters

It is interesting to see how surface instabilities caused by roughening (faceting) or by surface melting may be related to the observed shape transition of gold nanorods. To study such surface effects we first start by considering gold cluster cooled from a liquid.

By constant temperature MD, a liquid gold cluster with 2624 atoms initially at 1500K was cooled down to 100K step by step. We find that the cluster is formed with an icosahedral shape. Despite the little displacement of the outside atoms from their ideal positions, the atoms forming global icosahedral structure fall into three local-structure categories: the atoms in the tetrahedral units with fcc local structure, the atoms in the internal twinning palne with an hcp local symmetry, and the atoms on the line from the center to the surface vertices with a decahedral symmetry[10] (Fig. 6).

The icosahedral cluster is then heated up, with a temperature step of 100K, till 1500K (steps of 10K near melting temperature are used). At each temperature level, the system was equilibrated for 4.3ns and data were collected for the following 17.2ns. The caloric curve of potential energy (Fig. 7) shows the melting transition occurs at about

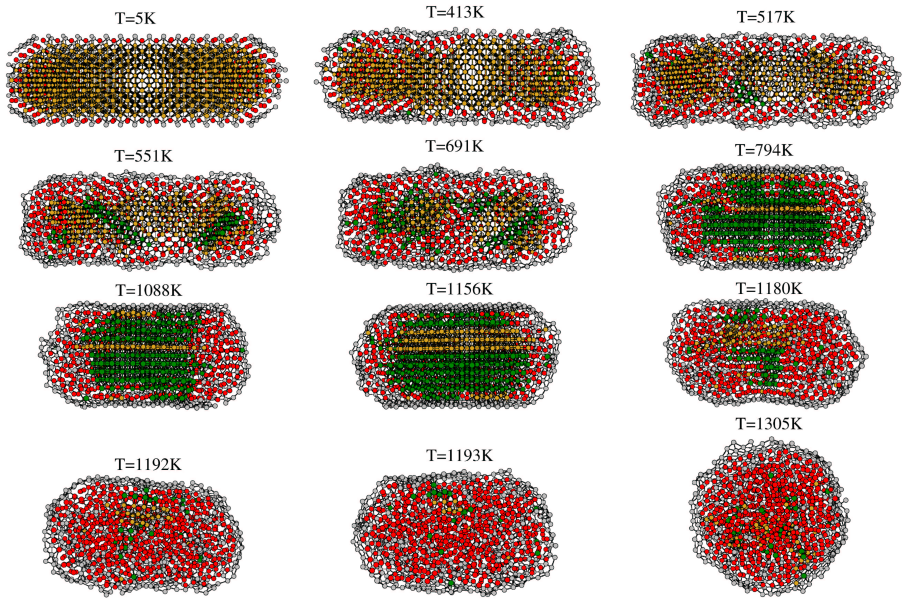

FIG. 5: Configurations of the 2624-atom gold nanorod at different temperatures with atoms colored according to their local structure. The configurations have been cut into half to allow a better view of the internal structures. Surface atoms are gray, amorphous atoms are red, fcc atoms are yellow, and hcp atoms are green.

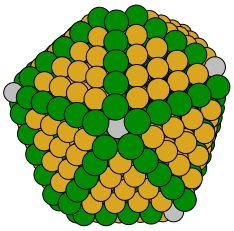

FIG. 6: The internal structure of an icosahedral gold cluster. The atoms with fcc local structure are colored as yellow, hcp as green, and decahedron as gray.

1090K. By using the cone algorithm recursively, each configuration of the gold cluster has been divided into six layers

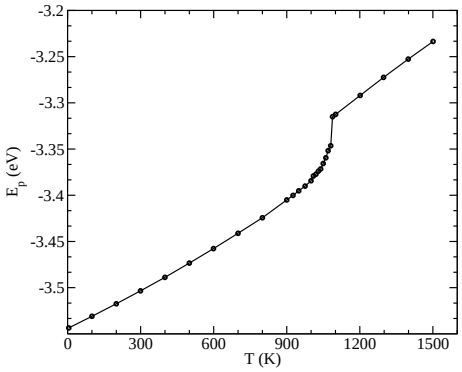

FIG. 7: Caloric curve of potential energy of icosahedral gold cluster with 2624 atoms.

and labeled 0-5, where layer 0 is the surface layer and layer 5 is the inside bulk. Mean squared displacement (Fig. 8), interlayer diffusion (Fig. 9), and bond order parameter measurements (Fig. 10) have been carried out for those layers.

Five hundred configurations have been saved for 17ns to calculate the mean squared displacements (Fig. 8). The atoms are labeled according to their initial layer numbers and do not relabel during the whole calculations. At

$T = 700$K, vetex atoms on the surface layer and the sub-surface layer start to hop around and diffuse into the other layer. At $T = 900$K, the vertex can travel longer distances and the edge atoms also diffuse. Surface layer and first sub-layer atoms already diffuse a lot at $T = 1000$K, which is quite below the melting temperature $T_m = 1090$K. The atoms on the other layers also have noticable movements. All of the atoms travel across the whole liquid cluster at $T = 1100$K, which is above the melting temperature.

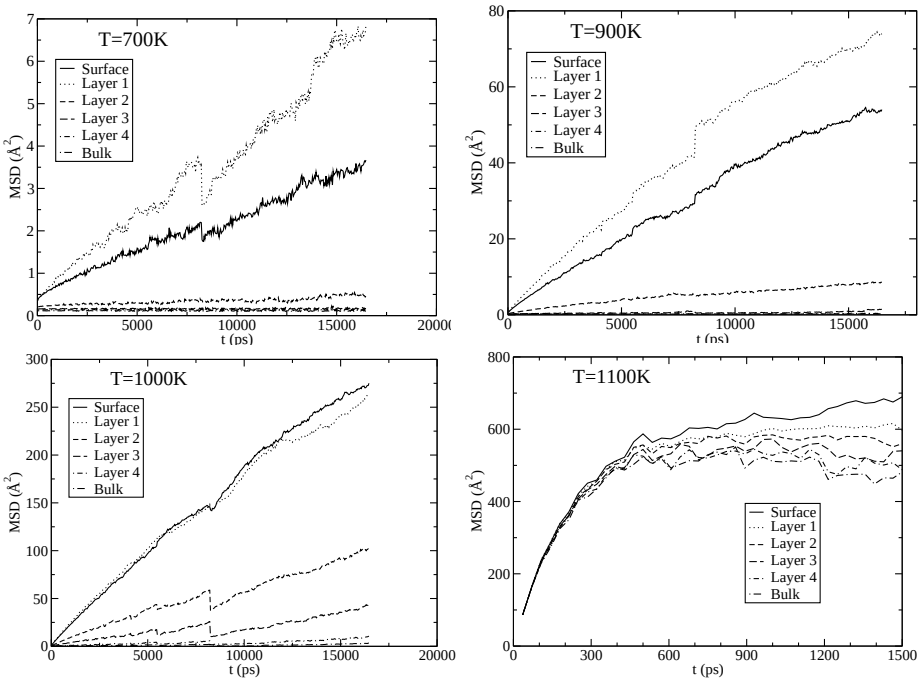

FIG. 8: Mean squared displacements of various layers at 700K, 900K, 1000K and 1100K.

Interlayer diffusion of atoms has also been analyzed to characterize the mobility of atoms traveling among layers. At each temperature, the atoms were labeled to the number of the layer they initially stay on. At the end of the simulation, the atoms were relabeled to the final layer numbers. The final numbers were averaged for each initial layer (Fig. 9). At $T = 700$K, the surface layer and the first sub-layer starts to exchange atoms around vertices. The sub-surface layer atoms then have the chance to go to the surface and diffuse, which have been shown in Fig. 8. At $T = 900$K, the vertex and edge atoms on the surface and sub-surface layers have significant exchange. At $T = 1050$K, all of the layers exchange some atoms with other layers. Above $T = 1100$K, all of the atoms have equal probability to be labeled as any layer numbers, which illustrates the liquid state in which all of the atoms travel freely across the whole cluster.

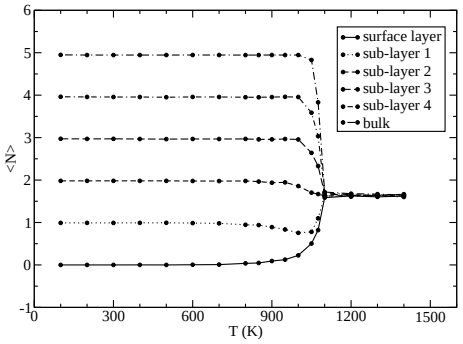

FIG. 9: Interlayer diffusion of atoms of the icosahedral gold cluster.

The average bond order parameters calculation was performed on the 2D structures for the surface layer, so the values are different from those of the bulk. In Fig. 10 we show the results for surface and bulk. For surface only bond angles between the surface atoms were included in average. Both plots again show that the melting temperature is a

little less than $T = 1100$K.

Unlike the mean squared displacements or the diffusion coefficients, the bond order parameters of the surface layer keep almost unchanged up to $T = 1000$K ($\hat{W}_4$ has so large error bars that it is invalid in this structure evaluation). This may imply that the surface structure is destroyed at much higher temperature than the onset temperature of the surface diffusion.

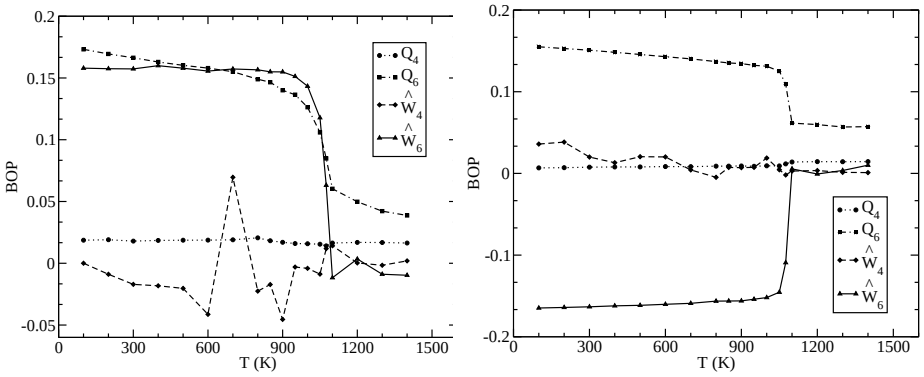

FIG. 10: The average bond order parameters for the surface layer (left) and the bulk (right) of the icosahedral gold cluster.

Each configuration at the end of the simulation went through further 4.3ns constant temperature MD to collect 100 configuraions, over which the atom positions have then been averaged to get the average shape at each temperature as shown in Fig. 11. The surface atoms of the avearage shape went through the local curvature fitting to get local curvature values. They were then colored with 10 color levels reflecting larger local parabolic curvatures ($-0.2\mathring{A}^{-1}$ - $0.6\mathring{A}^{-1}$), with warmer colors corresponding to larger curvature values.

We can see from those pictures that vertex atoms start to move around at the temperature as low as 600K. Because of the thermal movement and diffusion of the surface atoms, the vertices and edges get rounded at $T = 700$K and $T = 800$K and start to disappear at $T = 900$K. At $T = 1000$K, the vertices and edges totally disappear, but there are still some atoms on large facets remain unmoved.

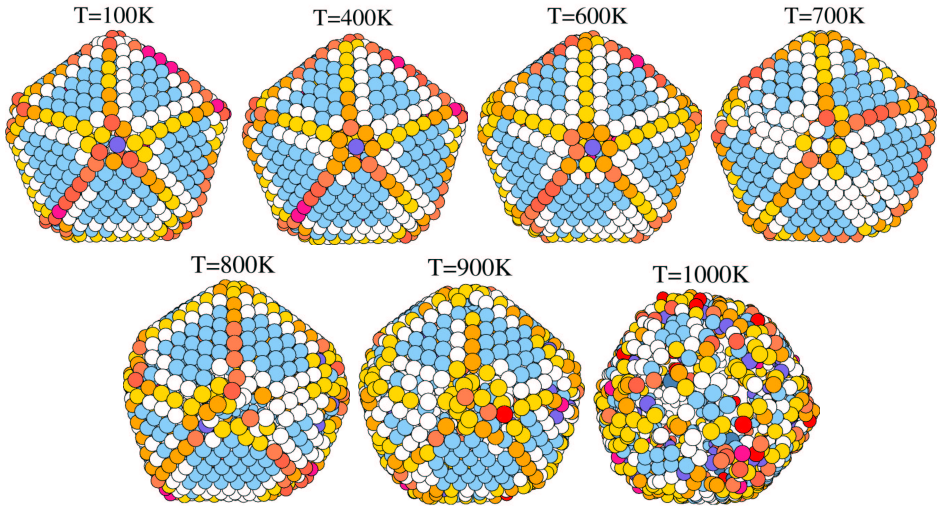

FIG. 11: Average shape of the gold cluster.

C. Faceting Transition of Gold Nanorods

Finally the methods developed for the icosahedral gold cluster have been applied on the configurations of the gold nanorod with 11076 atoms. The surface atoms were colored with the same method as for the icosahedral gold cluster.

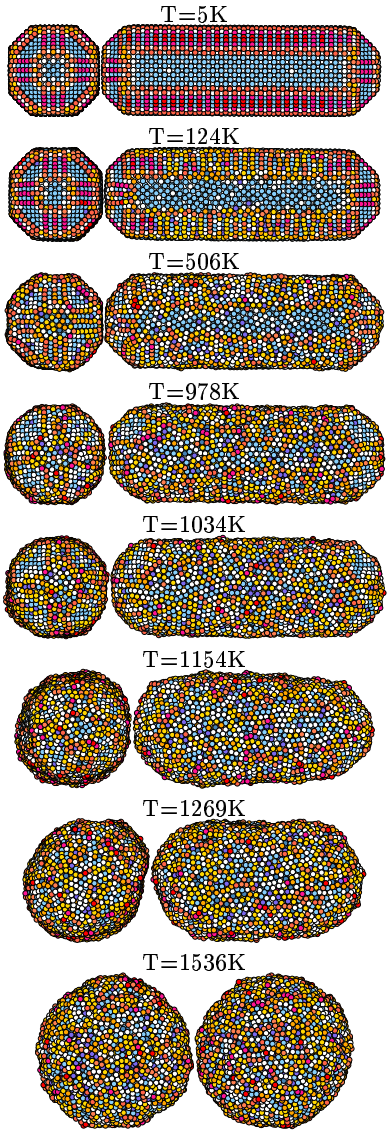

FIG. 12: Coloring of the surface atoms of the gold nanorods with 11076 atoms reflecting their larger local parabolic curvatures.

The onset temperature of shape transition is about 990K and that of melting transition is about 1280K. From Fig. 12 we can see qualitatively that the surface facets are closely related to the morphological change of the gold nanorod. Global shape change seems to appear only when the 100 facets along the long side of the rod dissapear. Further simuation and more detailed analysis are expected to quantify the relation between the faceting transition and the shape and melting transitions of gold nanorods.

IV. CONCLUSIONS

Continuous heating MD simulations of gold nanorods have revealed shape and melting transitions coincident with the observations in laser heating experiments of gold nanorods. Raising from these simulations was the interesting question of how the surface is geometrically and energetically enrolled in the morphological and structural change of gold nanorods. Detailed analysis of the melting procedure of icosahedral gold clusters provided the knowledge that the vertices, edges and facets get rounder with higher temperature and totally disappear below bulk melting temperature. By applying the analysis methods for the icosahedral gold clusters to the instantaneous configurations of the gold nanorod, it was qualitatively indicated that macroscopic shape transformations are intimately connected with the faceting transition occuring on the sides of the nanorod.

V. ACKNOWLEDGMENT

Many thanks to my advisors Prof. Stephen Teitel and Prof. Christoph Dellago for their great instructions and many helps.

---

[1] Wang, Y.; Dellago, C. *J. Phys. Chem. B* submitted (2003).
[2] Ercolessi, F.; Parrinello, M.; Tosatti, E. *Philos. Mag. A* **1988**, *58*, 213.
[3] Allen, M. P.; Tildesley, D. J. *Computer Simulation of Liquids*; Clarendon Press: Oxford, 1987.
[4] Steinhardt, P. J.; Nelson, D. R.; Ronchetti, M. *Phys. Rev. B* **1983**, *28*, 784.
[5] Landau, L. D.; Lifshitz, F. M. *Quantum Mechanics*; Pergamon: New York, 1965.
[6] Wang, Z. L.; Mohamed, M. B.; Link, S.; El-Sayed, M. A. *Surf. Sci.* **1999**, *440*, L809.
[7] Chang, S.; Shih, C.; Chen, C.; Lai, W.; Wang, C. R. C. *Langmuir* **1999**, *103*, 1165.
[8] Link, S.; Burda, C.; Nikoobakht, B.; El-Sayed, M. A. *J. Phys. Chem. B* **2000**, *104*, 6152.
[9] Link, S.; Wang, Z. L.; El-Sayed, M. A. *J. Phys. Chem. B* **2000**, *104*, 7867.
[10] Chushak, Y. G.; Bartell, L. S. *J. Phys. Chem. B* **2001**, *105*, 11605.